Eawag
Swiss Federal Institute of Aquatic Science and Technology

Spike
Sensor management, Process Intelligence and Control at Eawag

Technical Report No. 6, v3.0

(TR006030)

Extent-based Model Identification under Incomplete Observability Conditions

Authors (alphabetically):
Julien Billeter, Dominique Bonvin, Kris Villez

Dübendorf, Switzerland
Last update: 18/02/2019

Contents

1 Purpose and structure of this document

The main purpose of this document is to elaborate on a few variations on a method for incremental parameter estimation based on an extent framework dealing with rank deficient conditions. This version of the technical report is best read as an addendum to [1] as it is assumed that the reader is familiar with the methods therein. Early variations of this method can be found in [2, 3]. Additional information concerning extent-based method preceding this development can be found in [4, 5, 6, 7, 8, 9]

2 Notation and symbols

The notation and symbols in use are the same as in [1].

3 Methods

3.1 Observable and Unobservable Extent Directions via Singular Value Decomposition

{sec:svd}

The next paragraphs continue from the end of Section 3.2 in [1] and provide an alternative to the developments in sections 3.3 to 3.5.
A first variation of the method is obtained by considering an alternative factorization of the extent-based measurement gain matrix based on singular value decomposition (SVD). In the original work, $\mathbf{G}_{\bullet,\mathbf{a}}$ is factorized by means of the reduced-row echelon form (RREF). However, the same system partitioning would be obtained if $\mathbf{G}$ were factorized directly. When using SVD for decomposition, this is not the case anymore. This means two options are available:

(a) Factorization of $\mathbf{G}_{\bullet,\mathbf{a}}$. In this case, the RREF is used to define observable, ambiguous, and non-sensed extents. Then, the ambiguous extents are decomposed into observable and non-observable directions among them.

(b) Factorization of $\mathbf{G}$. In this case, the results of the RREF factorization are ignored and the SVD of $\mathbf{G}$ is used to define observable and non-observable direction among all extents.

In this report, only the second option is studied in detail. This is executed for two reasons:

(a) It enables demonstrating that SVD leads to uncorrelated estimation errors for all observable directions when $\mathbf{G}$ is factorized. This is not the case when using the factorization of $\mathbf{G}_{\bullet,\mathbf{a}}$.

(b) It enables demonstrating that SVD does not lead to optimal partitioning of the parameter estimation problem.

3.1.1 Factorization of G

{factor}

Let A be the rank of the $(M \times R)$-dimensional measurement matrix $\mathbf{G}$. Then, $\mathbf{G}$ can be factorized into the $(M \times A)$-dimensional measurement matrix $\overline{\boldsymbol{\mathcal{G}}}_\circ$ and the $(R \times A)$-dimensional matrix $\overline{\mathbf{V}}_\circ$:

$$\mathbf{G} = \overline{\boldsymbol{\mathcal{G}}}_\circ \, \overline{\mathbf{V}}_\circ{}^{\mathrm{T}}. \tag{1}$$ {factor10}

The matrices $\overline{\boldsymbol{\mathcal{G}}}_\circ$ and $\overline{\mathbf{V}}_\circ$ are computed via singular value decomposition of $\mathbf{G}$:

$$\mathbf{G} = \mathbf{U}\,\mathbf{S}\,\overline{\mathbf{V}}_\circ = \overline{\boldsymbol{\mathcal{G}}}_\circ \, \overline{\mathbf{V}}_\circ \tag{2}$$ {factor13}

3.1.2 Observable Extent Directions

We define the vector $\overline{\boldsymbol{\chi}}_\circ(t)$ consisting of the A observable directions among the extents as follows:

$$\overline{\boldsymbol{\chi}}_\circ(t) := \overline{\mathbf{V}}_\circ{}^{\mathrm{T}} \, \boldsymbol{x}(t). \tag{3}$$ {direct13}

With this definition, the measurement equation (Eq. 13 in [1]) can be rewritten as:

$$\tilde{\boldsymbol{y}}_h = \boldsymbol{y}_0 + \frac{1}{V} \, \overline{\boldsymbol{\mathcal{G}}}_\circ \, \overline{\boldsymbol{\chi}}_\circ(t_h) + \boldsymbol{\epsilon}_h.$$

Since the $(R \times A)$-dimensional matrix $\overline{\boldsymbol{\mathcal{G}}}_\circ$ has full column rank, one can compute the maximum-likelihood estimates $\tilde{\overline{\boldsymbol{\chi}}}_{\circ,h}$ of the observable extents and extent directions directly from the measurements:

$$\tilde{\overline{\boldsymbol{\chi}}}_{\circ,h} = \mathbf{P} \, (\tilde{\boldsymbol{y}}_h - \boldsymbol{y}_0) \; , \tag{4}$$ {comput10}

with the $(A \times M)$-dimensional matrix $\mathbf{P}$ given by:

$$\mathbf{P} = V \left(\overline{\boldsymbol{\mathcal{G}}}_{\mathsf{o}}{}^{\mathrm{T}} \, \boldsymbol{\Sigma}_{\epsilon}^{-1} \, \overline{\boldsymbol{\mathcal{G}}}_{\mathsf{o}} \right)^{-1} \overline{\boldsymbol{\mathcal{G}}}_{\mathsf{o}}{}^{\mathrm{T}} \, \boldsymbol{\Sigma}_{\epsilon}^{-1}. \tag{5}$$ {comput11}

The associated expected variance-covariance matrix of the estimation errors becomes:

$$\boldsymbol{\Sigma}_{\overline{\chi}} = \mathbf{P} \, \boldsymbol{\Sigma}_{\epsilon} \, \mathbf{P}^{\mathrm{T}} = \left(\overline{\boldsymbol{\mathcal{G}}}_{\mathsf{o}}{}^{\mathrm{T}} \, \boldsymbol{\Sigma}_{\epsilon}^{-1} \, \overline{\boldsymbol{\mathcal{G}}}_{\mathsf{o}} \right)^{-1}. \tag{6}$$ {comput12}

Remark 1. Since $\overline{\boldsymbol{\mathcal{G}}}_{\mathsf{o}}$ consists of orthonormal column vectors it follows that $\boldsymbol{\Sigma}_{\overline{\chi}}$ will be diagonal if $\boldsymbol{\Sigma}_{\epsilon}$ is diagonal, meaning that the estimation errors are uncorrelated.

3.1.3 Unobservable Extent Directions

The unobservable extent directions span the null space of $\mathbf{G}$, which is also the null space of $\overline{\mathbf{V}}_{\mathsf{o}}{}^{\mathrm{T}}$. Denoting this null space by the $(R \times (R-A))$-dimensional matrix $\overline{\mathbf{V}}_{\mathsf{u}}$,

$$\overline{\mathbf{V}}_{\mathsf{u}} := \mathsf{null} \left(\overline{\mathbf{V}}_{\mathsf{o}}{}^{\mathrm{T}} \right), \tag{7}$$

we define the vector $\overline{\boldsymbol{\chi}}_{\mathsf{u}}(t)$ consisting of the $R - A$ unobservable extents and non-sensed extent directions as follows:

$$\overline{\boldsymbol{\chi}}_{\mathsf{u}}(t) := \overline{\mathbf{V}}_{\mathsf{u}}{}^{\mathrm{T}} \, \boldsymbol{x}(t) \, . \tag{8}$$ {direct30}

With this definition, the expression for the number of moles (Eq. 12 in [1] can be rewritten as:

$$\boldsymbol{n}(t) = \boldsymbol{n}_0 + \overline{\boldsymbol{\mathcal{N}}}_{\mathsf{o}}{}^{\mathrm{T}} \, \overline{\boldsymbol{\chi}}_{\mathsf{o}}(t) + \overline{\boldsymbol{\mathcal{N}}}_{\mathsf{u}}{}^{\mathrm{T}} \, \overline{\boldsymbol{\chi}}_{\mathsf{u}}(t) \tag{9}$$ {direct31}

with:

$$\overline{\boldsymbol{\mathcal{N}}}_{\mathsf{o}} := \left(\overline{\mathbf{V}}_{\mathsf{o}} \right)^{+} \mathbf{N} \tag{10}$$ {direct32}

$$\overline{\boldsymbol{\mathcal{N}}}_{\mathsf{u}} := \left(\overline{\mathbf{V}}_{\mathsf{u}} \right)^{+} \mathbf{N} \tag{11}$$ {direct33}

3.2 Partitioning into subsystems with smallest number of parameters

{sec:partition}

An algorithm is developed to group the kinetic parameters into J parameter subsets ($j = 1, \ldots, J$), each represented as a $T^{(j)}$-dimensional vector $\boldsymbol{\theta}^{(j)}$ satisfying the following properties:

- The size $T^{(j)}$ of each parameter subset should be as small as possible.
- The estimates $\hat{\boldsymbol{\theta}}^{(j)}$ in the jth parameter subset can be computed without consideration of any other parameter subset $\boldsymbol{\theta}^{(i)}$, $i \neq j$.
- None of the parameter sets are a subset of any of the other parameter sets.

Note that the last property is different from the one presented in [1]. To account for this, we apply modifications in step 1 and 2 of the procedure. These are shown in blue. The original procedure is named *SI* (sharing infeasible). The newly proposed one is named *SP* (sharing permitted). We also explain the modifications necessary to account for the SVD-based decomposition described above and indicate these in red. Note that these modifications can be applied independently of each other, leading to four possible combined methods: SVD-SI, SVD-SP, RREF-SI (as in [1]), and RREF-SP.

3.2.1 Step 1—Model Reformulation

{Step1}

An extended model is first defined to describe the dynamics of all extents and all observable directions among the ambiguous extents. To this end, the following procedure is applied:

(a) Express $\dot{\boldsymbol{x}}(t)$ as a function of $\overline{\boldsymbol{\chi}}_{\mathsf{o}}(t)$ and $\boldsymbol{x}(t)$

The dynamic model (Eq. 6-8 in [1]) is modified by replacing $\boldsymbol{n}(t)$ with the right-hand side of (9):

$$\dot{\boldsymbol{x}}(t) = V\, \boldsymbol{f}\left(\overline{\boldsymbol{\chi}}_{\mathsf{o}}(t), \overline{\boldsymbol{\chi}}_{\mathsf{u}}(t), \boldsymbol{\theta}\right), \qquad \boldsymbol{x}(0) = \mathbf{0}. \tag{12}$$

{steponeA1}

The vector $\overline{\boldsymbol{\chi}}_{\mathsf{u}}(t)$ is now replaced with the right-hand side of (8). As a result, the above system becomes:

$$\dot{\boldsymbol{x}}(t) = V\, \boldsymbol{f}\left(\overline{\boldsymbol{\chi}}_{\mathsf{o}}(t), \boldsymbol{x}(t), \boldsymbol{\theta}\right), \qquad \boldsymbol{x}(0) = \mathbf{0}. \tag{13}$$

{steponeA2}

(b) State augmentation

Define the ρ_{aug}-dimensional vector $\boldsymbol{\chi}_{\mathsf{aug}}(t) := \begin{bmatrix} \boldsymbol{x}(t) \\ \overline{\boldsymbol{\chi}}_{\mathsf{o}}(t) \end{bmatrix} = \begin{bmatrix} \mathbf{I}_R \\ \overline{\mathbf{V}}_{\mathsf{o}}{}^{\mathrm{T}} \end{bmatrix} \boldsymbol{x}(t)$ that includes all extents and observable extent directions, with $\rho_{\mathsf{aug}} = R+A$. The dynamic behavior of $\boldsymbol{\chi}_{\mathsf{aug}}(t)$ can be described by a differential-algebraic system including the R differential equations (13) and the A algebraic expressions (3):

$$\dot{\boldsymbol{x}}(t) = V\, \boldsymbol{f}\left(\overline{\boldsymbol{\chi}}_{\mathsf{o}}(t), \boldsymbol{x}(t), \boldsymbol{\theta}\right) , \qquad \boldsymbol{x}(0) = \mathbf{0} \tag{14}$$ {steponeB1}

$$\overline{\boldsymbol{\chi}}_{\mathsf{o}}(t) = \overline{\mathbf{V}}_{\mathsf{o}}{}^{\mathrm{T}}\, \boldsymbol{x}(t) . \tag{15}$$ {steponeB2}

(c) Interpolation of the observable extents and extent directions

To increase the efficiency of system partitioning, it is useful to account for the fact that the observable extents and extent directions can be expressed in terms of measurements. However, since the observable extents and extent directions are only known at H discrete measurement points, their values always need to be obtained via interpolation. In this work, we apply piece-wise linear interpolation as follows:

$$\tilde{\overline{\boldsymbol{\chi}}}_{\mathsf{o,i}}(t) := \tilde{\overline{\boldsymbol{\chi}}}_{\mathsf{o},h} + \frac{t - t_h}{t_{h+1} - t_h} \left(\tilde{\overline{\boldsymbol{\chi}}}_{\mathsf{o},h+1} - \tilde{\overline{\boldsymbol{\chi}}}_{\mathsf{o},h}\right) , \quad t_h \le t < t_{h+1} , \quad h = 1, \ldots, H, \tag{16}$$ {comput20}

with which the system (14) and (15) becomes:

$$\dot{\boldsymbol{x}}(t) = V\, \boldsymbol{f}\left(\tilde{\overline{\boldsymbol{\chi}}}_{\mathsf{o,i}}(t), \boldsymbol{x}(t), \boldsymbol{\theta}\right) , \qquad \boldsymbol{x}(0) = \mathbf{0} \tag{17}$$ {steponeC1}

$$\overline{\boldsymbol{\chi}}_{\mathsf{o}}(t) = \overline{\mathbf{V}}_{\mathsf{o}}{}^{\mathrm{T}}\, \boldsymbol{x}(t) . \tag{18}$$ {steponeC2}

3.2.2 Step 2—Graph-Based System Partitioning

The equation system (17) and (18) is now analyzed by means of a graph partitioning procedure to determine the smallest groups of kinetic parameters that can be estimated separately while allowing that parameters appear in multiple sets. To this end, the following steps are performed:

(a) Create a graph

One creates a directed graph $\mathcal{F}$ with a vertex for every state variable in $\boldsymbol{\chi}_{\mathsf{aug}}(t)$ and every parameter in $\boldsymbol{\theta}$. Hence, this graph has $R + \rho_{\mathsf{o}} + T$

vertices. A directed arc is added from vertex v to vertex w if the vth element of $\left[\begin{smallmatrix}\boldsymbol{\chi}_{\mathsf{aug}}(t)\\ \boldsymbol{\theta}\end{smallmatrix}\right]$ appears in the right-hand side of the wth equation in (17) and (18) ($v = 1, \ldots, R + A + T$, $w = 1, \ldots, R + A$). This graph represents the information flow for simulating (17) and (18). Additional arcs and vertices may be added to describe the influence of known inputs and the links between extents and measured variables. For system partitioning, this is however unnecessary and omitted for clarity.

(b) Extents predicted from measurements or simulation
The simultaneous approach uses a complete model of the reaction system to predict the extents (or concentrations) via simulation. If one wants to partition the reaction system into small groups of reactions, only the extents belonging to a given group can be generated via the simulation of that group. The other extents that enter the rate laws must be provided by the user as quantities known from measurements.

That information can be included in the graph $\mathcal{F}$ by annotating the various arcs. The arcs that originate at a vertex corresponding to an observable extent or an observable extent direction are labeled *observation arcs*, considering that observable extent or an observable extent direction can be replaced with their measured values (16). They are visualized as dashed-line arrows. The remaining arcs are labeled *simulation arcs* and visualized as solid-line arrows. The observation arcs represent the idea that the elements of $\widetilde{\overline{\boldsymbol{\chi}}}_{\mathsf{o,i}}(t)$ can be regarded as known inputs for simulating (17) and (18).

(c) Subgraph selection
Identify the $J := A$ subgraphs $\mathcal{F}^{(j)}$ such that each of the subgraphs consists of arcs and vertices in $\mathcal{F}$ on directed paths that (i) lead to one of the A vertices representing an observable extent or an observable extent direction (ignore observable extents in the SVD case); and (ii) consist of simulation arcs only. The selected vertices represent an $R^{(j)}$-dimensional vector of extents $\boldsymbol{x}^{(j)}(t)$, a $\rho_{\mathsf{o}}^{(j)}$-dimensional vector of directions $\overline{\boldsymbol{\chi}}_{\mathsf{o}}^{(j)}(t)$, and a $T^{(j)}$-dimensional vector of parameters $\boldsymbol{\theta}^{(j)}$. The positions of $\boldsymbol{x}^{(j)}(t)$ in $\boldsymbol{x}(t)$ are given by the vector $\mathbf{j}$ so that:

$$\boldsymbol{x}^{(j)}(t) := \mathbf{I}_{\mathbf{j},\bullet}\, \boldsymbol{x}(t) \qquad (19) \quad \{\texttt{steptwoC11}\}$$

$$\boldsymbol{f}^{(j)}(\bullet) := \mathbf{I}_{\mathbf{j},\bullet}\, \boldsymbol{f}(\bullet)\,, \qquad (20) \quad \{\texttt{steptwoC12}\}$$

and the selection matrices $\mathbf{\Lambda}_{\mathbf{o}}^{(j)}$ and $\mathbf{\Lambda}_{\theta}^{(j)}$ are defined so that:

$$\overline{\boldsymbol{\chi}}_{\mathbf{o}}^{(j)}(t) := \mathbf{\Lambda}_{\mathbf{o}}^{(j)}\, \overline{\boldsymbol{\chi}}_{\mathbf{o}}(t) \qquad (21) \quad \{\texttt{steptwoC13}\}$$

$$\boldsymbol{\theta}^{(j)} := \mathbf{\Lambda}_{\theta}^{(j)}\, \boldsymbol{\theta}. \qquad (22) \quad \{\texttt{steptwoC14}\}$$

This means that each subgraph $\mathcal{F}^{(j)}$ represents a subset of Equations (17) and (18) that describes the dynamics of $\boldsymbol{x}^{(j)}(t)$ and $\boldsymbol{\chi}_{\mathbf{o}}^{(j)}(t)$ without reference to any other state variable:

$$\dot{\boldsymbol{x}}^{(j)}(t) = V\, \boldsymbol{f}^{(j)}\left(\tilde{\overline{\boldsymbol{\chi}}}_{\mathbf{o},\mathbf{i}}(t), \boldsymbol{x}^{(j)}(t), \boldsymbol{\theta}^{(j)}\right), \qquad \boldsymbol{x}^{(j)}(0) = \boldsymbol{x}_{\mathbf{o}} \qquad (23) \quad \{\texttt{steptwoC21}\}$$

$$\boldsymbol{\chi}_{\mathbf{o}}^{(j)}(t) = \mathbf{U}^{(j)}\, \boldsymbol{x}^{(j)}(t), \qquad (24) \quad \{\texttt{steptwoC22}\}$$

with $\mathbf{U}^{(j)} := \mathbf{\Lambda}_{\mathbf{o}}^{(j)}\, {\mathbf{V}_{\mathbf{o}}}^{\mathrm{T}}\, \mathbf{I}_{\mathbf{a},\bullet}\, {\mathbf{I}_{\mathbf{j},\bullet}}^{\mathrm{T}}$.

(d) Redundant subsets of equations

It is possible that one subset of equations exhibits a parameter vector which is included completely in the parameter vector of subset of equations. Three possible approaches to deal with this are feasible:

(a) Minimal overlap. Subsets of equations with parameter vectors included completely in the parameter vector of another subset of equations are merged into a single subset. This minimizes the number of parameter estimation problems that are solved.

(b) Sequential. Subsets of equations with the exact same parameter are merged. Then, the subsystems with parameter vectors included completely in the parameter vector of another subset of equations are used first during parameter estimation. The obtained values can function as an initial guess for the subset of equations with the larger parameter vector. This approach could also be useful for model diagnosis, e.g. to identify whether certain model components need an revised structure.

(c) One-by-one. The identified subsystems are left unmodified, even when there are subsystems with parameter vectors that are exactly the same. In this case, the number of subsystems will always equal the rank A of $\mathbf{G}$. The order in which the subsystems are used can be optimized to enable reuse of parameter estimates as initial guesses in subsequent parameter estimation problems.

In the present report, the first approach is applied.

(e) Add observation arcs and vertices

For every graph $\mathcal{F}^{(j)}$, add (i) the observation arcs that have a target vertex belonging to $\mathcal{F}^{(j)}$ and (ii) the source vertices of the added observation arcs. These added source vertices represent the minimal subset of interpolants in $\tilde{\overline{\boldsymbol{\chi}}}_{\mathsf{o},\mathsf{i}}(t)$ (16) that are required to simulate $\boldsymbol{x}^{(j)}(t)$ and $\boldsymbol{\chi}_{\mathsf{o}}^{(j)}(t)$ and are referred to as $\tilde{\overline{\boldsymbol{\chi}}}_{\mathsf{o},\mathsf{i}}^{(j)}(t)$. This means that the graph $\mathcal{F}^{(j)}$ now represents all information required to simulate the observable extents $\boldsymbol{x}^{(j)}(t)$ and the observable extent directions $\boldsymbol{\chi}_{\mathsf{o}}^{(j)}(t)$. Accordingly, one can rewrite the jth equation subsystem as:

$$\dot{\boldsymbol{x}}^{(j)}(t) = V\, \boldsymbol{f}^{(j)}\left(\tilde{\overline{\boldsymbol{\chi}}}_{\mathsf{o},\mathsf{i}}^{(j)}(t), \boldsymbol{\chi}_{\mathsf{o}}^{(j)}(t), \boldsymbol{x}^{(j)}(t), \boldsymbol{\theta}^{(j)}\right), \quad \boldsymbol{x}^{(j)}(0) = \boldsymbol{x}_{\mathbf{o}} \tag{25}$$ {steptwoD1}

$$\boldsymbol{\chi}_{\mathsf{o}}^{(j)}(t) = \mathbf{U}^{(j)}\, \boldsymbol{x}^{(j)}(t). \tag{26}$$ {steptwoD2}

At the end of this procedure, the equation system (17) and (18) is approximated by J smaller equation subsystems, each including a subset of the kinetic parameters. As intended, every kinetic parameter appears in at most one of the J subsystems. In addition, the identified subsystems do not share any of the observable extents or extent directions as state variables, that is, each observable extent and extent direction is simulated in only one of the identified subsystems.

3.3 Parameter Estimation Methods

The applicable parameter estimation methods are exactly the same as in [1]. In this report, we do not solve the parameter estimation problems but restrict ourselves to a discussion of the partitioning results.

3.4 Implementation

All results can be reproduced with the open-source Efficient Model Identification (EMI) MATLAB package (v4.1) for efficient model identification [8] that is extended to include all methods and simulations used in this study. At the time of writing, this package can be found on Gitlab at this location: `https://gitlab.com/krisvillez/emi`.

4 Results

The methods are demonstrated with a small toy example, deliberately designed to demonstrate observed challenges with the newly obtained methods.

4.1 Example

This reaction system has $R = 5$ reactions involving $S = 4$ species (A to D) with the following reaction scheme:

$$\begin{array}{lrcrcrcl} R_1: & \mathrm{A} + & \mathrm{B} & \longrightarrow & \mathrm{C} & & & \\ R_2: & 2\,\mathrm{A} + & 2\,\mathrm{B} & \longrightarrow & 2\,\mathrm{C} & & & \\ R_3: & \mathrm{A} & & \longrightarrow & \mathrm{C} & & & \\ R_4: & & \mathrm{B} & \longrightarrow & \mathrm{C} & & & \\ R_5: & & & & \mathrm{C} & \longrightarrow & \mathrm{D} & \end{array}$$

with

$$\mathbf{N} := \begin{bmatrix} -1 & -1 & +2 & 0 \\ -2 & -2 & +4 & 0 \\ -1 & 0 & +1 & 0 \\ 0 & -1 & +1 & 0 \\ 0 & 0 & -1 & +1 \end{bmatrix}. \tag{27}$$ {ex11}

4.1.1 Dynamic Model in Terms of Numbers of Moles

The simulated kinetic rate expressions are:

$$\boldsymbol{f}\left(\boldsymbol{n}(t), \boldsymbol{\theta}\right) := \begin{bmatrix} \frac{k_1}{V^2}\,\left(n_1(t)\,n_2(t) - K_1\,V\,n_3(t)\right) \\ \frac{k_2}{V^4}\,n_1(t)^2\,n_2(t)^2 \\ \frac{k_3}{V}\,n_1(t) \\ \frac{k_4}{V}\,\left(n_2(t) - K_4\,n_3(t)\right) \\ \frac{k_5}{V}\,n_3(t)^2 \end{bmatrix} \tag{28}$$ {ex12}

with $\boldsymbol{\theta} := \begin{bmatrix} k_1 & k_2 & k_3 & k_4 & k_5 & K_1 & K_4 \end{bmatrix}^{\mathrm{T}}$.
We assume all concentrations are measured, that is,

$$\mathbf{M} := \mathbf{I}_4. \tag{29}$$

4.1.2 Extent labeling

It follows that $\mathbf{G}$ equals:

$$\mathbf{G} = \mathbf{M}\,\mathbf{N}^{\mathrm{T}} = \begin{bmatrix} -1 & -2 & -1 & 0 & 0 \\ -1 & -2 & 0 & -1 & 0 \\ +2 & +4 & +1 & +1 & -1 \\ 0 & 0 & 0 & 0 & +1 \end{bmatrix}. \tag{30}$$

The reduced row echelon form of $\mathbf{G}$ is

$$\mathbf{B} = \begin{bmatrix} +1 & +2 & 0 & +1 & 0 \\ 0 & 0 & +1 & -1 & 0 \\ 0 & 0 & 0 & 0 & +1 \\ 0 & 0 & 0 & 0 & 0 \end{bmatrix}, \tag{31}$$

which indicates that there are:

- $R_{\mathsf{n}} = 0$ non-sensed extents,
- $R_{\mathsf{o}} = 1$ observable extent, $\boldsymbol{x}_{\mathbf{o}}(t) = x_5(t)$,
- $R_{\mathsf{a}} = 4$ ambiguous extents, $\boldsymbol{x}_{\mathbf{a}}(t) = \begin{bmatrix} x_1(t) & x_2(t) & x_3(t) & x_4(t) \end{bmatrix}^{\mathrm{T}}$,

which gives:

$$\mathbf{G}_{\bullet,\mathbf{a}} = \begin{bmatrix} -1 & -2 & -1 & 0 \\ -1 & -2 & 0 & -1 \\ +2 & +4 & +1 & +1 \\ 0 & 0 & 0 & 0 \end{bmatrix}. \tag{32}$$

4.1.3 Method 1 – SVD-SI

Observable and Unobservable Extent Directions We start with the SVD-SI method. This means the methods in Section 3.1 are used and the modifications indicated in red in Section 3.2 are applied [1].

SVD factorization of $\mathbf{G}$ leads to:

$$\overline{\boldsymbol{\mathcal{G}}}_{\circ} = \begin{bmatrix} 2.3199 & -0.3433 & -0.7071 \\ 2.3199 & -0.3433 & 0.7071 \\ -4.7863 & -0.3026 & 0 \\ 0.1464 & 0.9892 & 0 \end{bmatrix}, \tag{33}$$

$$\overline{\mathbf{V}}_{\circ}{}^{\mathrm{T}} = \begin{bmatrix} -0.4218 & -0.8436 & -0.2109 & -0.2109 & +0.1464 \\ +0.0624 & +0.1248 & +0.0312 & +0.0312 & +0.9892 \\ 0 & 0 & +0.7071 & -0.7071 & 0 \end{bmatrix}, \tag{34}$$

so that

$$\begin{aligned} \boldsymbol{\chi}_{\circ}(t) &= \overline{\mathbf{V}}_{\circ}{}^{\mathrm{T}} \boldsymbol{x}(t) \\ &= \begin{bmatrix} -0.4218 & -0.8436 & -0.2109 & -0.2109 & +0.1464 \\ +0.0624 & +0.1248 & +0.0312 & +0.0312 & +0.9892 \\ 0 & 0 & +0.7071 & -0.7071 & 0 \end{bmatrix} \boldsymbol{x}(t) \end{aligned} \tag{35}$$

$$\overline{\boldsymbol{\chi}}_{\circ}(t) = \begin{bmatrix} \boldsymbol{x}(t) \\ \boldsymbol{\chi}_{\circ}(t) \end{bmatrix}. \tag{36}$$

The values of the observable extents and extent directions $\tilde{\overline{\boldsymbol{\chi}}}_{\circ,h} := \begin{bmatrix} \tilde{x}_{5,h} & \tilde{\chi}_{\circ,1,h} & \tilde{\chi}_{\circ,2,h} \end{bmatrix}^{\mathrm{T}}$ can be computed from (4) with

$$\mathbf{P} = \begin{bmatrix} +0.0689 & +0.0689 & -0.1421 & +0.0043 \\ -0.2629 & -0.2629 & -0.2317 & +0.7575 \\ -0.7071 & +0.7071 & 0 & 0 \end{bmatrix}. \tag{37}$$

With $\boldsymbol{\Sigma}_{\epsilon} = \mathbf{I}_4\, 10^{-4}\,\mathrm{mol}^2\mathrm{L}^{-2}$, the expected estimation error variance-covariance matrix $\boldsymbol{\Sigma}_{\overline{\chi}}$ is:

$$\boldsymbol{\Sigma}_{\overline{\chi}} = \begin{bmatrix} 0.0297 & 0 & 0 \\ 0 & 0.7658 & 0 \\ 0 & 0 & 1.0000 \end{bmatrix} 10^{-4}. \tag{38}$$

A clear advantage of the SVD decomposition is therefore that the estimation errors in the computed extent directions are uncorrelated.

Expression (9) is then specified with the following vectors and matrices:

$$\overline{\boldsymbol{\mathcal{N}}}_{\mathsf{o}} := \begin{bmatrix} +\alpha_1 & +\alpha_1 & -\alpha_4 & +\alpha_6 \\ -\alpha_2 & -\alpha_2 & -\alpha_5 & +\alpha_7 \\ -\alpha_3 & +\alpha_3 & 0 & 0 \end{bmatrix} \tag{39}$$

$$= \begin{bmatrix} +2.3199 & +2.3199 & -4.7863 & +0.1464 \\ -0.3433 & -0.3433 & -0.3026 & +0.9892 \\ -0.7071 & +0.7071 & 0 & 0 \end{bmatrix}. \tag{40}$$

$$\overline{\boldsymbol{\mathcal{N}}}_{\mathsf{u}} := \mathbf{0}_{5\times 4} \tag{41}$$

System partitioning Following Steps 1(a)-(b) in Section 3.2.1 (with SVD-related modifications, in red above), the augmented equation system becomes:

$$\dot{\boldsymbol{x}} = \begin{bmatrix} \frac{k_1}{V^2}\left[\left(n_{0,1}+\alpha_1\,\tilde{\chi}_{\mathsf{o},1}-\alpha_2\,\tilde{\chi}_{\mathsf{o},2}-\alpha_3\,\tilde{\chi}_{\mathsf{o},3}\right)\dots \right. \\ \qquad \dots\left(n_{0,2}+\alpha_1\,\tilde{\chi}_{\mathsf{o},1}-\alpha_2\,\tilde{\chi}_{\mathsf{o},2}+\alpha_3\,\tilde{\chi}_{\mathsf{o},3}\right)\dots \\ \qquad\qquad \left.\dots - K_1\,V\,\left(n_{0,3}-\alpha_4\,\tilde{\chi}_{\mathsf{o},1}-\alpha_5\,\tilde{\chi}_{\mathsf{o},2}\right)\right] \\ \frac{k_2}{V^4}\,\left(n_{0,1}+\alpha_1\,\tilde{\chi}_{\mathsf{o},1}-\alpha_2\,\tilde{\chi}_{\mathsf{o},2}-\alpha_3\,\tilde{\chi}_{\mathsf{o},3}\right)^2\dots \\ \qquad \dots\left(n_{0,2}+\alpha_1\,\tilde{\chi}_{\mathsf{o},1}-\alpha_2\,\tilde{\chi}_{\mathsf{o},2}+\alpha_3\,\tilde{\chi}_{\mathsf{o},3}\right)^2 \\ \qquad \frac{k_3}{V}\,\left(n_{0,1}+\alpha_1\,\tilde{\chi}_{\mathsf{o},1}-\alpha_2\,\tilde{\chi}_{\mathsf{o},2}-\alpha_3\,\tilde{\chi}_{\mathsf{o},3}\right) \\ \frac{k_4}{V}\left[\left(n_{0,2}+\alpha_1\,\tilde{\chi}_{\mathsf{o},1}-\alpha_2\,\tilde{\chi}_{\mathsf{o},2}+\alpha_3\,\tilde{\chi}_{\mathsf{o},3}\right)\dots \right. \\ \qquad\qquad \left.\dots - K_4\,\left(n_{0,3}-\alpha_4\,\tilde{\chi}_{\mathsf{o},1}-\alpha_5\,\tilde{\chi}_{\mathsf{o},2}\right)\right] \\ \qquad \frac{k_5}{V}\,\left(n_{0,3}-\alpha_4\,\tilde{\chi}_{\mathsf{o},1}-\alpha_5\,\tilde{\chi}_{\mathsf{o},2}\right)^2 \end{bmatrix}, \qquad \boldsymbol{x}\,(0) = \mathbf{0} \tag{42}$$

$$\boldsymbol{\chi}_{\mathsf{o}} = \begin{bmatrix} -0.4218 & -0.8436 & -0.2109 & -0.2109 & +0.1464 \\ +0.0624 & +0.1248 & +0.0312 & +0.0312 & +0.9892 \\ 0 & 0 & +0.7071 & -0.7071 & 0 \end{bmatrix} \boldsymbol{x}(t). \tag{43}$$

Figure 1 shows the graph corresponding to the above equation system. The vertices corresponding to the observable extents and extent direction are shaded, while the other vertices are white. The simulation arcs are shown with full-line arrows, while the observation arcs are shown as dashed-line arrows. To identify possible subsystems, one removes all the observation arcs, as shown in Figure 2. In this case, one can only identify a single subsystem, meaning that the SVD-SI method is an ineffective approach to divide the parameter estimation problem into smaller problems.

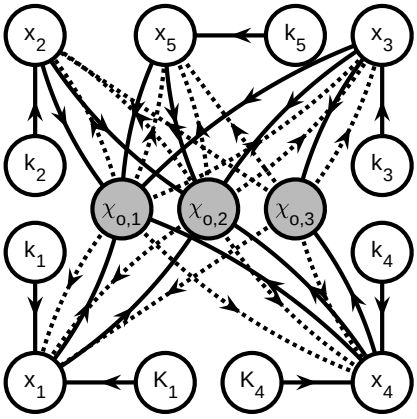

Figure 1: Method 1—Graph $\mathcal{F}$. There are three shaded vertices corresponding the observable extent directions ($\chi_{o,1}$, $\chi_{o,2}$, $\chi_{o,3}$). The remaining vertices represent the extents (x_1, x_2, x_3, x_4, and x_5) and the parameters (k_1, k_2, k_3, k_4, k_5, K_1, K_4). The simulation and observation arcs are shown as solid-line and dashed-line arrows, respectively. {fig:method1:graph

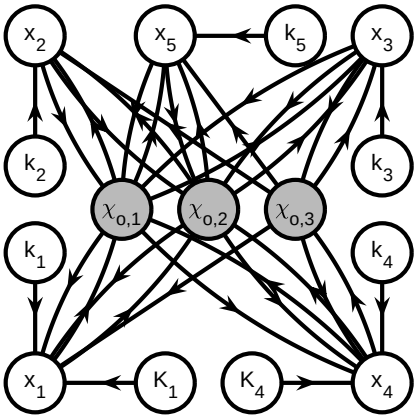

Figure 2: Method 1—Graph $\mathcal{F}$ without observation arcs. Removing the observation arcs from $\mathcal{F}$ and graph partitioning results in a single subgraph for all parameters. {fig:method1:graph

4.1.4 Method 2 – SVD-SP

We continue with the SVD-SP method. This means the methods in Section 3.1 are used and all modifications (red and blue) indicated in Section 3.2 are applied. In this case, all results are exactly the same as with the SVD-SI method up to the generation of $\mathcal{F}$ as shown in Figure 3 .

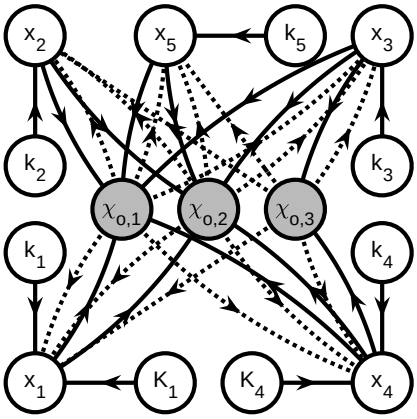

Figure 3: Method 2—Graph $\mathcal{F}$. There are three shaded vertices corresponding the observable extent directions ($\chi_{o,1}$, $\chi_{o,2}$, $\chi_{o,3}$). The remaining vertices represent the extents (x_1, x_2, x_3, x_4, and x_5) and the parameters (k_1, k_2, k_3, k_4, k_5, K_1, K_4). The simulation and observation arcs are shown as solid-line and dashed-line arrows, respectively. {fig:method2:graph

Applying the partitioning method shown above leads to three subgraphs at the end of Step 2c. These are shown in Figure 4-6
Applying Step 2d means that each of these subgraphs are joined together into one graph again. This is because all parameter vertices in subgraph 2 and 3 are also parameter vertices in subgraph 1. Consequently, the SVD-SP method is ineffective as a way to separate the original parameter estimation problem into smaller problems. However, and as indicated above, an alternative strategy could consist of estimating the parameters k_3, k_4, and K_4 by first solving the parameter estimation problem corresponding to subgraph 3, followed by estimation of all parameters using the available estimates for k_3, k_4, and K_4 as initial guesses.

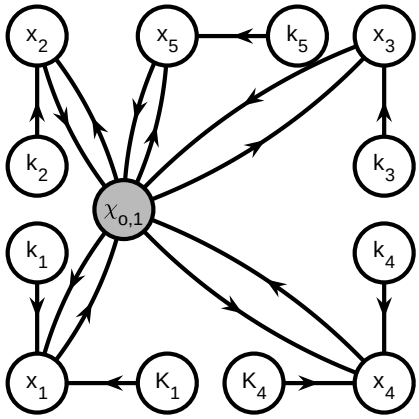

Figure 4: Method 2— Subgraph 1. Removing the observation arcs from $\mathcal{F}$ and finding paths to the vertex for $\chi_{o,1}$ results in a subgraph in which all parameters (k_1, k_2, k_3, k_4, K_1, and K_4) are connected to the observable quantity $\chi_{o,1}$. {fig:method2:graph

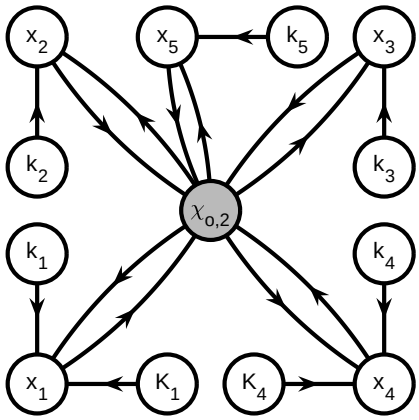

Figure 5: Method 2— Subgraph 2. Removing the observation arcs from $\mathcal{F}$ and finding paths to the vertex for $\chi_{o,2}$ results in a subgraph in which all parameters (k_1, k_2, k_3, k_4, K_1, and K_4) are connected to the observable quantity $\chi_{o,2}$. {fig:method2:graph

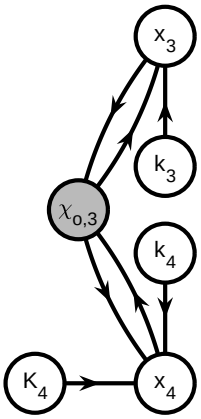

Figure 6: Method 2— Subgraph 3. Removing the observation arcs from $\mathcal{F}$ and finding paths to the vertex for $\chi_{o,3}$ results in a subgraph in which the parameters k_3, k_4, and K_4 are connected to the observable quantity $\chi_{o,3}$. {fig:method2:graph

4.1.5 Method 3 – RREF-SI

Observable and Unobservable Extent Directions We now apply the RREF-SI method. This is the exact method represented in [1].
The factorization of $\mathbf{G}_{\bullet,\mathbf{a}}$ gives:

$$\boldsymbol{\mathcal{G}}_{\circ} = \begin{bmatrix} -1 & -1 \\ -1 & 0 \\ +2 & +1 \\ 0 & 0 \end{bmatrix}, \qquad \mathbf{V}_{\circ}{}^{\mathrm{T}} = \begin{bmatrix} +1 & +2 & 0 & 1 \\ 0 & 0 & +1 & -1 \end{bmatrix}, \tag{44}$$

so that

$$\boldsymbol{\chi}_{\circ}(t) = \mathbf{V}_{\circ}{}^{\mathrm{T}}\, \mathbf{I}_{\mathbf{a},\bullet}\, \boldsymbol{x}(t) = \begin{bmatrix} +1 & +2 & 0 & +1 & 0 \\ 0 & 0 & +1 & -1 & 0 \end{bmatrix} \boldsymbol{x}(t) \tag{45}$$

$$= \begin{bmatrix} x_1(t) + 2\,x_2(t) + x_4(t) \\ x_3(t) - x_4(t) \end{bmatrix} \tag{46}$$

$$\overline{\boldsymbol{\chi}}_{\circ}(t) = \begin{bmatrix} x_5(t) \\ x_1(t) + 2\,x_2(t) + x_4(t) \\ x_3(t) - x_4(t) \end{bmatrix}. \tag{47}$$

The values of the observable extents and extent directions $\tilde{\overline{\boldsymbol{\chi}}}_{\circ,h} := \begin{bmatrix} \tilde{x}_{5,h} & \tilde{\chi}_{\circ,1,h} & \tilde{\chi}_{\circ,2,h} \end{bmatrix}^{\mathrm{T}}$ can be computed from (4) with

$$\mathbf{P} = \begin{bmatrix} -\frac{1}{4} & -\frac{1}{4} & -\frac{1}{4} & +\frac{3}{4} \\ +\frac{1}{4} & -\frac{3}{4} & +\frac{1}{4} & +\frac{1}{4} \\ -1 & +1 & 0 & 0 \end{bmatrix}. \tag{48}$$

With $\boldsymbol{\Sigma}_{\epsilon} = \mathbf{I}_4\, 10^{-4}\,\mathrm{mol}^2\mathrm{L}^{-2}$, the expected estimation error variance-covariance matrix $\boldsymbol{\Sigma}_{\overline{\chi}}$ is:

$$\boldsymbol{\Sigma}_{\overline{\chi}} = \begin{bmatrix} +3 & +1 & 0 \\ +1 & +3 & -4 \\ 0 & -4 & +8 \end{bmatrix} \frac{1}{4}\, 10^{-4}. \tag{49}$$

Expression (9) is then specified with the following vectors and matrices:

$$\overline{\boldsymbol{\mathcal{N}}}_{\circ} := \begin{bmatrix} 0 & 0 & -1 & +1 \\ -1 & -1 & +2 & 0 \\ -1 & 0 & +1 & 0 \end{bmatrix}. \tag{50}$$

$$\overline{\boldsymbol{\mathcal{N}}}_{\mathsf{u}} := \mathbf{0}_{5\times 4} \tag{51}$$

System partitioning Following Steps 1(a)-(b) in Section 3.2.1 (without modifications, as in [1]), the augmented equation system becomes:

$$\dot{\boldsymbol{x}} = \begin{bmatrix} \frac{k_1}{V^2}\left[\left(n_{0,1}-\tilde{\chi}_{\mathrm{o},1}-\tilde{\chi}_{\mathrm{o},2}\right)\left(n_{0,2}-\tilde{\chi}_{\mathrm{o},1}\right)\dots\right. \\ \left.\dots - K_1\, V\,\left(n_{0,3}-\tilde{x}_5+2\,\tilde{\chi}_{\mathrm{o},1}+\tilde{\chi}_{\mathrm{o},2}\right)\right] \\ \frac{k_2}{V^4}\,\left(n_{0,1}-\tilde{\chi}_{\mathrm{o},1}-\tilde{\chi}_{\mathrm{o},2}\right)^2\,\left(n_{0,2}-\tilde{\chi}_{\mathrm{o},1}\right)^2 \\ k_3\left(n_{0,1}-\tilde{\chi}_{\mathrm{o},1}-\tilde{\chi}_{\mathrm{o},2}\right) \\ \frac{k_4}{V}\left[\left(n_{0,2}-\tilde{\chi}_{\mathrm{o},1}\right)\dots\right. \\ \left.\dots - K_4\,\left(n_{0,3}-\tilde{x}_5+2\,\tilde{\chi}_{\mathrm{o},1}+\tilde{\chi}_{\mathrm{o},2}\right)\right] \\ \frac{k_5}{V^2}\,\left(n_{0,3}-\tilde{x}_5+2\,\tilde{\chi}_{\mathrm{o},1}+\tilde{\chi}_{\mathrm{o},2}\right)^2 \end{bmatrix}, \quad \boldsymbol{x}\left(0\right)=\mathbf{0} \tag{52}$$

$$\boldsymbol{\chi}_{\mathrm{o}} = \begin{bmatrix} x_1+2\,x_2+x_4 \\ x_3-\,x_4 \end{bmatrix}. \tag{53}$$

Figure 7 shows the graph corresponding to the above equation system. The vertices corresponding to the observable extents and extent direction are shaded, while the other vertices are white. The simulation arcs are shown with full-line arrows, while the observation arcs are shown as dashed-line arrows. To identify possible subsystems, one removes all the observation arcs, which results in two subgraphs as shown in Figure 8. The first subgraph includes the parameters k_1, k_2, k_3, k_4, K_1, and K_4, which affect the observable quantities $\chi_{\mathrm{o},1}$ and $\chi_{\mathrm{o},2}$ via a network that also involves the unobservable extents x_1, x_2, x_3, and x_4. The second subgraph is much smaller and includes the parameter k_5 that influences the observable extent x_5. Consequently, this graph partitioning enables splitting the parameter estimation problem into two smaller parameter estimation problems. One to estimate k_1, k_2, k_3, k_4, K_1, and K_4 and one to estimate k_5. The solutions are computed with the EMI toolbox (not shown).

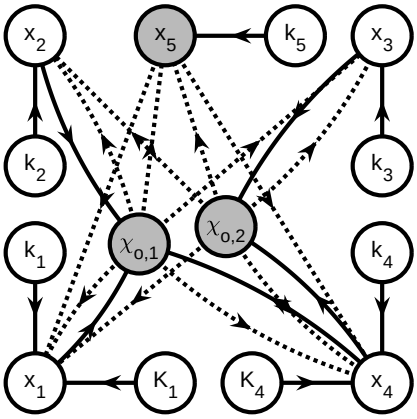

Figure 7: Method 3—Graph $\mathcal{F}$. There are three shaded vertices corresponding the observable extent (x_5) and extent directions ($\chi_{o,1}$, $\chi_{o,2}$). The remaining vertices represent the unobservable extents (x_1, x_2, x_3, and x_4) and the parameters (k_1, k_2, k_3, k_4, k_5, K_1, K_4). The simulation and observation arcs are shown as solid-line and dashed-line arrows, respectively. {fig:method3:graph

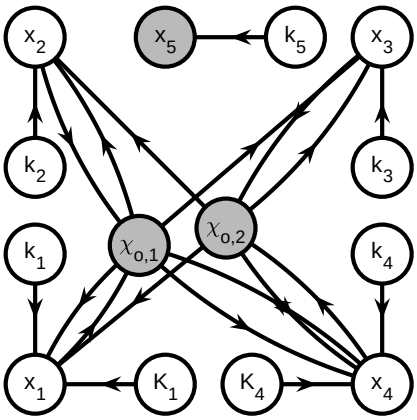

Figure 8: Method 3—Graph $\mathcal{F}$ without observation arcs. Removing the observation arcs from $\mathcal{F}$ and graph partitioning results in 2 subgraphs for the parameters as shown in the inset: one graph in which k_1, k_2, k_3, k_4, K_1, and K_4 are connected to the observable quantities $\chi_{o,1}$ and $\chi_{o,2}$, and another graph in which k_5 is connected to the observable extent x_5. {fig:method3:graph

4.1.6 Method 4 – RREF-SP

We now apply the RREF-SP method. This means the methods in [1] are used except for the modifications indicated in blue in Section 3.2. In this case, all results are exactly the same up to the generation of $\mathcal{F}$ as shown in Figure 9 .

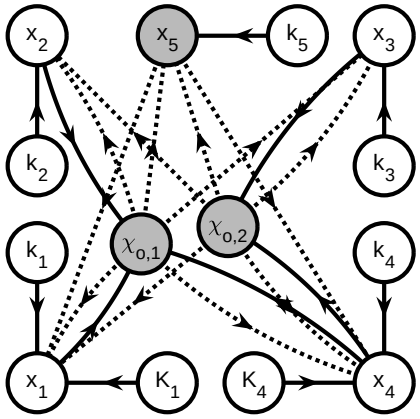

Figure 9: Method 4—Graph $\mathcal{F}$. There are three shaded vertices corresponding the observable extent (x_5) and extent directions ($\chi_{o,1}$, $\chi_{o,2}$). The remaining vertices represent the unobservable extents (x_1, x_2, x_3, and x_4) and the parameters (k_1, k_2, k_3, k_4, k_5, K_1, K_4). The simulation and observation arcs are shown as solid-line and dashed-line arrows, respectively. {fig:method4:graph

Applying the partitioning method shown above leads to three subgraphs at the end of Step 2c. These are shown in Figure 10-12
Applying Step 2d has no effect in this case. This is because each of the subgraphs include at least one parameter vertex which does not appear in any of the other subgraphs. Consequently, this graph partitioning enables splitting the parameter estimation problem into three smaller parameter estimation problems with 1, 3, and 5 parameters. One to estimate k_5, one to estimate k_1, k_2, k_4, K_1, and K_4 and one to estimate k_3, k_4, and K_4. This also means k_4 and K_4 are estimated twice. The solutions are computed with the EMI toolbox (not shown).

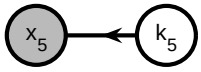

Figure 10: Method 4— Subgraph 1. Removing the observation arcs from $\mathcal{F}$ and finding paths to the vertex for $\chi_{o,1}$ results in a subgraph in which the parameter k_5 is connected to the observable quantity x_5. {fig:method4:graph

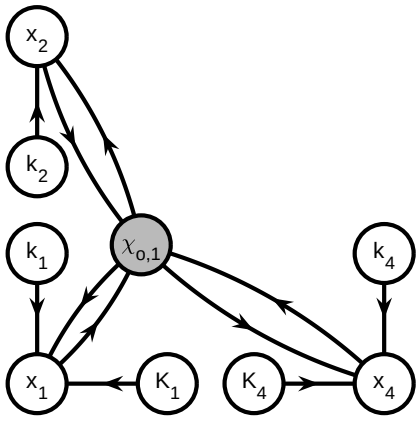

Figure 11: Method 4— Subgraph 2. Removing the observation arcs from $\mathcal{F}$ and finding paths to the vertex for $\chi_{o,2}$ results in a subgraph in which the parameters k_1, k_2, k_4, K_1, and K_4 are connected to the observable quantity $\chi_{o,1}$. {fig:method4:graph

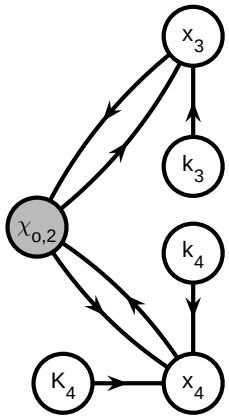

Figure 12: Method 4— Subgraph 3. Removing the observation arcs from $\mathcal{F}$ and finding paths to the vertex for $\chi_{o,3}$ results in a subgraph in which the parameters k_3, k_4, and K_4 are connected to the observable quantity $\chi_{o,2}$. {fig:method4:graph

4.2 Example – Alternative system representation 1

We now apply the RREF-SP method again to the same example studied above. However, we change the order in which the reactions are represented. Concretely, we swap the order of the 3rd and 4th reaction in the 4th and 3rd position prior to analysis. This means $\mathbf{N}$ and $\boldsymbol{f}(\bullet)$ are modified as follows:

$$\mathbf{N} := \begin{bmatrix} -1 & -1 & +2 & 0 \\ -2 & -2 & +4 & 0 \\ 0 & -1 & +1 & 0 \\ -1 & 0 & +1 & 0 \\ 0 & 0 & -1 & +1 \end{bmatrix} \tag{54}$$ {ex11alt1}

$$\boldsymbol{f}(\boldsymbol{n}(t), \boldsymbol{\theta}) := \begin{bmatrix} \frac{k_1}{V^2}\,(n_1(t)\,n_2(t) - K_1\,V\,n_3(t)) \\ \frac{k_2}{V^4}\,n_1(t)^2\,n_2(t)^2 \\ \frac{k_4}{V}\,(n_2(t) - K_4\,n_3(t)) \\ \frac{k_3}{V}\,n_1(t) \\ \frac{k_5}{V}\,n_3(t)^2 \end{bmatrix} \tag{55}$$ {ex12alt1}

Everything else is the same as before.

4.2.1 Extent labeling

It follows that $\mathbf{G}$ equals:

$$\mathbf{G} = \mathbf{M}\,\mathbf{N}^{\mathrm{T}} = \begin{bmatrix} -1 & -2 & 0 & -1 & 0 \\ -1 & -2 & -1 & 0 & 0 \\ +2 & +4 & +1 & +1 & -1 \\ 0 & 0 & 0 & 0 & +1 \end{bmatrix}. \tag{56}$$

The reduced row echelon form of $\mathbf{G}$ is

$$\mathbf{B} = \begin{bmatrix} +1 & +2 & 0 & +1 & 0 \\ 0 & 0 & +1 & -1 & 0 \\ 0 & 0 & 0 & 0 & +1 \\ 0 & 0 & 0 & 0 & 0 \end{bmatrix}, \tag{57}$$

which delivers the same labelling as before.

It follows that:

$$\mathbf{G}_{\bullet,\mathbf{a}} = \begin{bmatrix} -1 & -2 & 0 & -1 \\ -1 & -2 & -1 & 0 \\ +2 & +4 & +1 & +1 \\ 0 & 0 & 0 & 0 \end{bmatrix}. \tag{58}$$

4.2.2 Method 4 – RREF-SP

We now apply the RREF-SP method as before.

Observable and Unobservable Extent Directions The factorization of $\mathbf{G}_{\bullet,\mathbf{a}}$ gives:

$$\boldsymbol{\mathcal{G}}_{\mathbf{o}} = \begin{bmatrix} -1 & 0 \\ -1 & -1 \\ +2 & +1 \\ 0 & 0 \end{bmatrix}, \qquad \mathbf{V}_{\mathbf{o}}{}^{\mathrm{T}} = \begin{bmatrix} +1 & +2 & 0 & +1 \\ 0 & 0 & +1 & -1 \end{bmatrix}, \tag{59}$$

so that

$$\boldsymbol{\chi}_{\mathbf{o}}(t) = \mathbf{V}_{\mathbf{o}}{}^{\mathrm{T}}\,\mathbf{I}_{\mathbf{a},\bullet}\,\boldsymbol{x}(t) = \begin{bmatrix} +1 & +2 & 0 & +1 & 0 \\ 0 & 0 & +1 & -1 & 0 \end{bmatrix} \boldsymbol{x}(t) \tag{60}$$

$$= \begin{bmatrix} x_1(t) + 2\,x_2(t) + x_3(t) \\ x_4(t) - x_3(t) \end{bmatrix} \tag{61}$$

$$\overline{\boldsymbol{\chi}}_{\mathbf{o}}(t) = \begin{bmatrix} x_5(t) \\ x_1(t) + 2\,x_2(t) + x_3(t) \\ x_4(t) - x_3(t) \end{bmatrix}. \tag{62}$$

The values of the observable extents and extent directions $\tilde{\overline{\boldsymbol{\chi}}}_{\mathbf{o},h} := \begin{bmatrix} \tilde{x}_{5,h} & \tilde{\chi}_{\mathbf{o},1,h} & \tilde{\chi}_{\mathbf{o},2,h} \end{bmatrix}^{\mathrm{T}}$ can be computed from (4) with

$$\mathbf{P} = \begin{bmatrix} -\frac{1}{4} & -\frac{1}{4} & -\frac{1}{4} & +\frac{3}{4} \\ -\frac{3}{4} & +\frac{1}{4} & +\frac{1}{4} & +\frac{1}{4} \\ +1 & -1 & 0 & 0 \end{bmatrix}. \tag{63}$$

With $\boldsymbol{\Sigma}_{\epsilon} = \mathbf{I}_4\,10^{-4}\,\mathrm{mol}^2\mathrm{L}^{-2}$, the expected estimation error variance-covariance matrix $\boldsymbol{\Sigma}_{\overline{\chi}}$ is:

$$\boldsymbol{\Sigma}_{\overline{\chi}} = \begin{bmatrix} +3 & +1 & 0 \\ +1 & +3 & -4 \\ 0 & -4 & +8 \end{bmatrix} \frac{1}{4}\,10^{-4}. \tag{64}$$

Expression (9) is then specified with the following vectors and matrices:

$$\overline{\boldsymbol{\mathcal{N}}}_{\mathsf{o}} := \begin{bmatrix} 0 & 0 & -1 & +1 \\ -1 & -1 & +2 & 0 \\ 0 & -1 & +1 & 0 \end{bmatrix}. \tag{65}$$

$$\overline{\boldsymbol{\mathcal{N}}}_{\mathsf{u}} := \mathbf{0}_{5\times 4} \tag{66}$$

System partitioning Following Steps 1(a)-(b) in Section 3.2.1 (without modifications, as in [1]), the augmented equation system becomes:

$$\dot{\boldsymbol{x}} = \begin{bmatrix} \frac{k_1}{V^2}\left[\left(n_{0,1}-\tilde{\chi}_{\mathsf{o},1}\right)\left(n_{0,2}-\tilde{\chi}_{\mathsf{o},1}-\tilde{\chi}_{\mathsf{o},2}\right)\dots \right. \\ \left. \dots - K_1 V\left(n_{0,3}-\tilde{x}_5+2\,\tilde{\chi}_{\mathsf{o},1}+\tilde{\chi}_{\mathsf{o},2}\right)\right] \\ \frac{k_2}{V^4}\left(n_{0,1}-\tilde{\chi}_{\mathsf{o},1}\right)^2\left(n_{0,2}-\tilde{\chi}_{\mathsf{o},1}-\tilde{\chi}_{\mathsf{o},2}\right)^2 \\ \frac{k_4}{V}\left[\left(n_{0,2}-\tilde{\chi}_{\mathsf{o},1}-\tilde{\chi}_{\mathsf{o},2}\right)\dots \right. \\ \left. \dots - K_4\left(n_{0,3}-\tilde{x}_5+2\,\tilde{\chi}_{\mathsf{o},1}+\tilde{\chi}_{\mathsf{o},2}\right)\right] \\ \frac{k_3}{V}\left(n_{0,1}-\tilde{\chi}_{\mathsf{o},1}\right) \\ \frac{k_5}{V}\left(n_{0,3}-\tilde{x}_5+2\,\tilde{\chi}_{\mathsf{o},1}+\tilde{\chi}_{\mathsf{o},2}\right)^2 \end{bmatrix}, \quad \boldsymbol{x}(0) = \mathbf{0} \tag{67}$$

$$\boldsymbol{\chi}_{\mathsf{o}} = \begin{bmatrix} x_1 + 2\,x_2 + x_3 \\ x_4 - x_3 \end{bmatrix}. \tag{68}$$

Figure 13 shows the graph corresponding to the above equation system. The vertices corresponding to the observable extents and extent direction are shaded, while the other vertices are white. The simulation arcs are shown with full-line arrows, while the observation arcs are shown as dashed-line arrows.

Applying the partitioning method shown above leads to three subgraphs at the end of Step 2c. These are shown in Figure 14-16

Applying Step 2d has no effect in this case. This is because each of the subgraphs include at least one parameter vertex which does not appear in any of the other subgraphs. Consequently, this graph partitioning enables splitting the parameter estimation problem into three smaller parameter estimation problems with 1, 3, and 4 parameters. n this case, only 1 parameter (k_3) is estimated twice. The solutions are computed with the EMI toolbox (not shown).

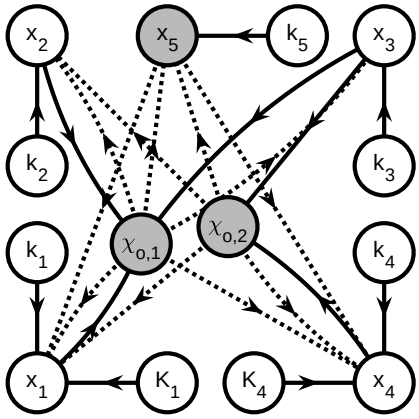

Figure 13: Method 4—Graph $\mathcal{F}$ for alternative representation 1. There are three shaded vertices corresponding the observable extent (x_5) and extent directions ($\chi_{o,1}$, $\chi_{o,2}$). The remaining vertices represent the unobservable extents (x_1, x_2, x_3, and x_4) and the parameters (k_1, k_2, k_3, k_4, k_5, K_1, K_4). The simulation and observation arcs are shown as solid-line and dashed-line arrows, respectively. {fig:alt1method4:g

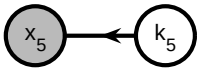

Figure 14: Method 4— Subgraph 1 for alternative representation 1. Removing the observation arcs from $\mathcal{F}$ and finding paths to the vertex for $\chi_{o,1}$ results in a subgraph in which the parameter k_5 is connected to the observable quantity x_5. {fig:alt1method4:g

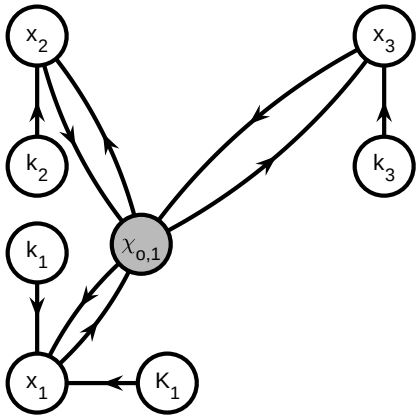

Figure 15: Method 4— Subgraph 2 for alternative representation 1. Removing the observation arcs from $\mathcal{F}$ and finding paths to the vertex for $\chi_{o,2}$ results in a subgraph in which the parameters k_1, k_2, k_3, and K_1 are connected to the observable quantity $\chi_{o,1}$. {fig:alt1method4:g

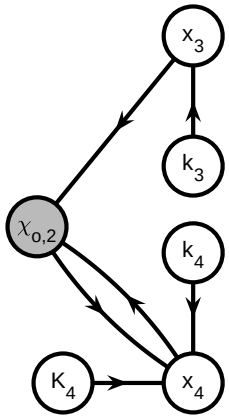

Figure 16: Method 4— Subgraph 3 for alternative representation 1. Removing the observation arcs from $\mathcal{F}$ and finding paths to the vertex for $\chi_{o,3}$ results in a subgraph in which the parameters k_3, k_4, and K_4 are connected to the observable quantity $\chi_{o,2}$. {fig:alt1method4:g

4.3 Example – Alternative system representation 2

We now apply the RREF-SP method again to the same example studied above. However, we change the order once more. This time, we reverse the order of the first four reactions prior to analysis. This means $\mathbf{N}$ and $\boldsymbol{f}(\bullet)$ are modified as follows:

$$\mathbf{N} := \begin{bmatrix} 0 & -1 & +1 & 0 \\ -1 & 0 & +1 & 0 \\ -2 & -2 & +4 & 0 \\ -1 & -1 & +2 & 0 \\ 0 & 0 & -1 & +1 \end{bmatrix} \tag{69}$$ {ex11alt2}

$$\boldsymbol{f}(\boldsymbol{n}(t), \boldsymbol{\theta}) := \begin{bmatrix} \frac{k_4}{V}\,(n_2(t) - K_4\, n_3(t)) \\ \frac{k_3}{V}\, n_1(t) \\ \frac{k_2}{V^4}\, n_1(t)^2\, n_2(t)^2 \\ \frac{k_1}{V^2}\,(n_1(t)\, n_2(t) - K_1\, V\, n_3(t)) \\ \frac{k_5}{V}\, n_3(t)^2 \end{bmatrix} \tag{70}$$ {ex12alt2}

Everything else is the same as before.

4.3.1 Extent labeling

It follows that $\mathbf{G}$ equals:

$$\mathbf{G} = \mathbf{M}\,\mathbf{N}^{\mathrm{T}} = \begin{bmatrix} 0 & -1 & -2 & -1 & 0 \\ -1 & 0 & -2 & -1 & 0 \\ +1 & +1 & +4 & +2 & -1 \\ 0 & 0 & 0 & 0 & +1 \end{bmatrix}. \tag{71}$$

The reduced row echelon form of $\mathbf{G}$ is

$$\mathbf{B} = \begin{bmatrix} +1 & 0 & +2 & +1 & 0 \\ 0 & +1 & +2 & +1 & 0 \\ 0 & 0 & 0 & 0 & +1 \\ 0 & 0 & 0 & 0 & 0 \end{bmatrix}, \tag{72}$$

which delivers the same labeling as before.

It follows that:

$$\mathbf{G}_{\bullet,\mathbf{a}} = \begin{bmatrix} 0 & -1 & -2 & -1 \\ -1 & 0 & -2 & -1 \\ +1 & +1 & +4 & +2 \\ 0 & 0 & 0 & 0 \end{bmatrix}. \tag{73}$$

4.3.2 Method 4 – RREF-SP

We now apply the RREF-SP method as before.

Observable and Unobservable Extent Directions The factorization of $\mathbf{G}_{\bullet,\mathbf{a}}$ gives:

$$\boldsymbol{\mathcal{G}}_{\mathbf{o}} = \begin{bmatrix} 0 & -1 \\ -1 & 0 \\ +1 & +1 \\ 0 & 0 \end{bmatrix}, \qquad \mathbf{V}_{\mathbf{o}}{}^{\mathrm{T}} = \begin{bmatrix} +1 & 0 & +2 & +1 \\ 0 & +1 & +2 & +1 \end{bmatrix}, \tag{74}$$

so that

$$\boldsymbol{\chi}_{\mathbf{o}}(t) = \mathbf{V}_{\mathbf{o}}{}^{\mathrm{T}}\,\mathbf{I}_{\mathbf{a},\bullet}\,\boldsymbol{x}(t) = \begin{bmatrix} +1 & 0 & +2 & +1 & 0 \\ 0 & +1 & +2 & +1 & 0 \end{bmatrix} \boldsymbol{x}(t) \tag{75}$$

$$= \begin{bmatrix} x_4(t) + 2\,x_2(t) + x_1(t) \\ x_3(t) + 2\,x_2(t) + x_1(t) \end{bmatrix} \tag{76}$$

$$\overline{\boldsymbol{\chi}}_{\mathbf{o}}(t) = \begin{bmatrix} x_5(t) \\ x_4(t) + 2\,x_2(t) + x_1(t) \\ x_3(t) + 2\,x_2(t) + x_1(t) \end{bmatrix}. \tag{77}$$

The values of the observable extents and extent directions $\tilde{\overline{\boldsymbol{\chi}}}_{\mathbf{o},h} := \begin{bmatrix} \tilde{x}_{5,h} & \tilde{\chi}_{\mathbf{o},1,h} & \tilde{\chi}_{\mathbf{o},2,h} \end{bmatrix}^{\mathrm{T}}$ can be computed from (4) with

$$\mathbf{P} = \begin{bmatrix} -\frac{1}{4} & -\frac{1}{4} & -\frac{1}{4} & +\frac{3}{4} \\ +\frac{1}{4} & -\frac{3}{4} & +\frac{1}{4} & +\frac{1}{4} \\ -3 & +1 & +1 & +1 \end{bmatrix}. \tag{78}$$

With $\boldsymbol{\Sigma}_{\epsilon} = \mathbf{I}_4\,10^{-4}\,\mathrm{mol}^2\mathrm{L}^{-2}$, the expected estimation error variance-covariance matrix $\boldsymbol{\Sigma}_{\overline{\chi}}$ is:

$$\boldsymbol{\Sigma}_{\overline{\chi}} = \begin{bmatrix} +3 & +1 & +1 \\ +1 & +3 & -1 \\ +1 & -1 & +8 \end{bmatrix} \frac{1}{4}\,10^{-4}. \tag{79}$$

Expression (9) is then specified with the following vectors and matrices:

$$\overline{\boldsymbol{\mathcal{N}}}_{\mathsf{o}} := \begin{bmatrix} 0 & 0 & -1 & +1 \\ 0 & -1 & +1 & 0 \\ -1 & 0 & +1 & 0 \end{bmatrix}. \tag{80}$$

$$\overline{\boldsymbol{\mathcal{N}}}_{\mathsf{u}} := \mathbf{0}_{5\times 4} \tag{81}$$

System partitioning Following Steps 1(a)-(b) in Section 3.2.1 (without modifications, as in [1]), the augmented equation system becomes:

$$\dot{\boldsymbol{x}} = \begin{bmatrix} \frac{k_4}{V}\left[\,(n_{0,2}-\tilde{\chi}_{\mathsf{o},1}) - K_4\,(n_{0,3}-\tilde{x}_5+\tilde{\chi}_{\mathsf{o},1}+\tilde{\chi}_{\mathsf{o},2})\,\right] \\ \frac{k_3}{V}\,(n_{0,1}-\tilde{\chi}_{\mathsf{o},2}) \\ \frac{k_2}{V^4}\,(n_{0,1}-\tilde{\chi}_{\mathsf{o},2})^2\,(n_{0,2}-\tilde{\chi}_{\mathsf{o},1})^2 \\ \frac{k_1}{V^2}\left[\,(n_{0,1}-\tilde{\chi}_{\mathsf{o},2})\,(n_{0,2}-\tilde{\chi}_{\mathsf{o},1}) - K_1\,V\,(n_{0,3}-\tilde{x}_5+\tilde{\chi}_{\mathsf{o},1}+\tilde{\chi}_{\mathsf{o},2})\,\right] \\ \frac{k_5}{V}\,(n_{0,3}-\tilde{x}_5+\tilde{\chi}_{\mathsf{o},1}+\tilde{\chi}_{\mathsf{o},2})^2 \end{bmatrix}, \quad \boldsymbol{x}\,(0) = \mathbf{0} \tag{82}$$

$$\boldsymbol{\chi}_{\mathsf{o}} = \begin{bmatrix} x_4 + 2\,x_2 + x_1 \\ x_3 + 2\,x_2 + x_1 \end{bmatrix}. \tag{83}$$

Figure 17 shows the graph corresponding to the above equation system. The vertices corresponding to the observable extents and extent direction are shaded, while the other vertices are white. The simulation arcs are shown with full-line arrows, while the observation arcs are shown as dashed-line arrows.

Applying the partitioning method shown above leads to three subgraphs at the end of Step 2c. These are shown in Figure 14-20.

Applying Step 2d has no effect in this case. This is because each of the subgraphs include at least one parameter vertex which does not appear in any of the other subgraphs. Consequently, this graph partitioning enables splitting the parameter estimation problem into three smaller parameter estimation problems with 1, 4, and 5 parameters. n this case, 3 parameters (k_1, k_2, and K_1) are estimated twice. The solutions are computed with the EMI toolbox (not shown).

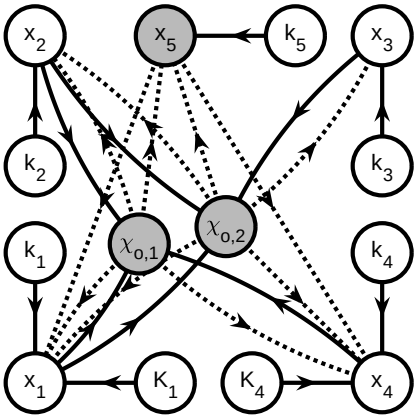

Figure 17: Method 4—Graph $\mathcal{F}$ for alternative representation 2. There are three shaded vertices corresponding the observable extent (x_5) and extent directions ($\chi_{o,1}$, $\chi_{o,2}$). The remaining vertices represent the unobservable extents (x_1, x_2, x_3, and x_4) and the parameters (k_1, k_2, k_3, k_4, k_5, K_1, K_4). The simulation and observation arcs are shown as solid-line and dashed-line arrows, respectively. {fig:alt2method4:g

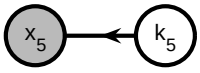

Figure 18: Method 4— Subgraph 1 for alternative representation 2. Removing the observation arcs from $\mathcal{F}$ and finding paths to the vertex for x_5 results in a subgraph in which the parameter k_5 is connected to the observable quantity x_5. {fig:alt2method4:g

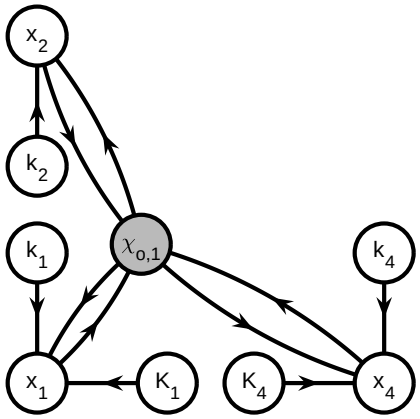

Figure 19: Method 4— Subgraph 2 for alternative representation 2. Removing the observation arcs from $\mathcal{F}$ and finding paths to the vertex for $\chi_{o,1}$ results in a subgraph in which the parameters k_1, k_2, k_4, K_1, and K_4 are connected to the observable quantity $\chi_{o,1}$. {fig:alt2method4:g

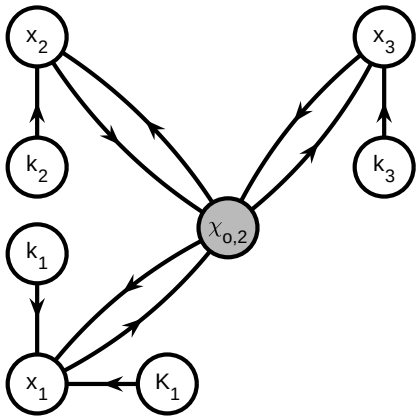

Figure 20: Method 4— Subgraph 3 for alternative representation 2. Removing the observation arcs from $\mathcal{F}$ and finding paths to the vertex for $\chi_{o,2}$ results in a subgraph in which the parameters k_1, k_2, k_3, and K_1 are connected to the observable quantity $\chi_{o,2}$. {fig:alt2method4:g

4.4 Example – Screening alternative representations

As a final result, we enumerate all permutations of the order of first 4 reactions and apply it to the example prior to analysis. There are therefore 24 possible presentations of the same example. We then apply the RREF-SP method and investigate the partitioning result by inspecting the subsystems to which each parameter belongs to.
The results are shown in Figure 21. Depending on the chosen permutation, one obtains 1 of 3 distinct partitioning results:

(a) 4 permutations lead to subsystems with parameter set *(i)* k_5; *(ii)* k_1, K_1, k_2, and k_3; and *(iii)* k_1, K_1, k_2, and K_4. k_1, K_1, and k_2 are thus estimated twice.

(b) 10 permutations lead to subsystems with parameter set *(i)* k_5; *(ii)* k_1, K_1, k_2, k_4, and K_4; and *(iii)* k_3, k_4, and K_4. k_4 and K_4 are thus estimated twice.

(c) 10 permutations lead to subsystems with parameter set *(i)* k_5; *(ii)* k_1, K_1, k_2, and k_3; and *(iii)* k_3, k_4, and K_4. k_3 is thus estimated twice.

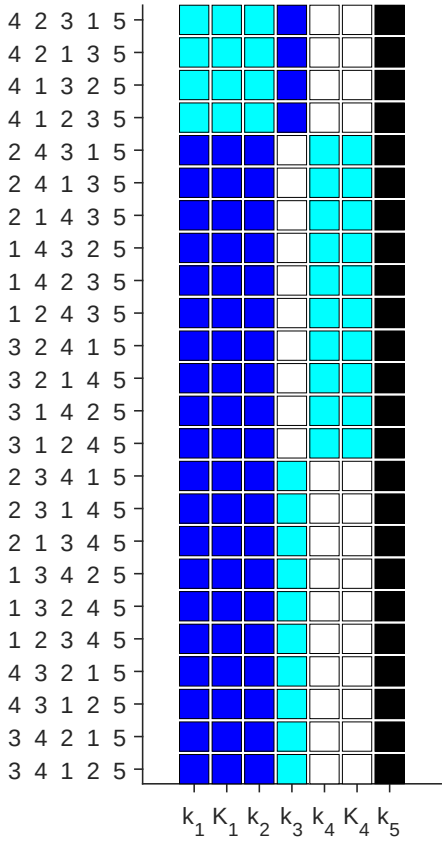

Figure 21: Method 4—Partitioning results for the seven parameters and for every permutation of the order of the first 4 reactions. Black, dark blue, and white are used for parameters belonging exclusively to subsystem 1, 2, and 3. Parameters belonging to subsystem 2 and 3 simultaneously are shown with light blue. One can see that the chosen permutation affects the obtained subsystem partitioning result. {fig:permute}

5 Discussion

5.1 Summary

This technical report explores a number of variations of the method for incremental parameter estimation presented in [1]. These variations include:

(a) A variation in which the computed extents and extent directions are defined via singular value decomposition (SVD) rather than the reduced row echelon form (RREF).

(b) A variation in which the system partitioning procedure is set up so to obtain smaller parameter sets compared to the original method (sharing infeasible, SI), in particular by allowing that a number of parameters appear in multiple subsystems (sharing permitted, SP).

The main results for the SVD variation are that:

(a) SVD, instead of RREF, enables to compute extent directions whose estimation errors are uncorrelated.

(b) Unfortunately, SVD leads to sub-optimal partitioning results, regardless of the applied partitioning procedure.

This means that applying SVD may produce tangible benefits when using the extent framework for process monitoring, including state estimation, and data reconciliation. Beneficial use for parameter estimation is expected to be limited.
The main results for the proposed SP variation are that:

(a) The SP variation permit to estimate parameters separately in a larger number of parameter sets which are smaller in size.

(b) Unfortunately, the partitioning result is not unique for a given system and depends on the order in which reactions are represented in the stoichiometric matrix ($\mathbf{N}$) and the vector-valued rate function ($\boldsymbol{f}$). Suggestions for improvement are discussed below.

5.2 Definitions of optimality

This technical report demonstrates that the utility of a given method for extent computation and partitioning depends on the definition of optimality. For example, SVD-based methods may be optimal for estimation but are sub-optimal for system partitioning. The same holds for the partitioning procedures as is discussed next.
In this study, we have assumed that the numbers of parameters that ought to be estimated simultaneously is a proper definition of optimality for system partitioning. One can easily challenge this notion of optimality. For example, there exist specialized methods which can separate parameters into parameters that appear linearly in the model predictions and parameters that appear non-linearly [10, 11]. One may therefore argue that the parameters that appear linearly in the model predictions should weigh much less when deciding between candidate partitions into subsystems. Once more, the exact definition of optimality may depend strongly on the exact application one has in mind.

5.3 Outlook – Optimal alternative to the SP procedure

To obtain a variation of the partitioning procedure which allows to split the parameter estimation problem in such a way that the subsystems contain the smallest number of parameters while allowing that a minimal number of parameters is estimated multiple times, we propose two additional variations of the partitioning procedure. These have not been tested yet:

- SM1. The RREF-SP method is modified as follows:

  I. The RREF is used to group the extents into clusters according to the subspace clustering paradigm of [12, 13]. Clusters consisting of one element are labeled observable. Extents not present in any cluster are non-sensed. The remaining clusters represent the ambiguous extents, grouped into one or more *clusters of ambiguous extents*. The columns of the extent-based measurement gain matrix corresponding to the extents in the kth cluster are used for form the matrix $\mathbf{G}_{\mathsf{a},k}$.

  II. For each cluster k:

  (a) Enumerate all order permutations of the reactions in this cluster.

(b) For each permutation, order the columns in $\mathbf{G}_{\mathsf{a},k}$ according the considered permutation and apply the SP partitioning procedure

(c) Select the permutation of the reactions which delivers an optimal partitioning, e.g. the smallest number of parameter in each subsystem and define the incremental parameter estimation procedure with these subsystems.

- SM2. The RREF-SP method is modified to avoid the exhaustive search in Step II.c of SM1. The SM2 method, if available, is expected to become practically relevant for cases where the clusters of ambiguous extents become so large that evaluating the partitioning results for every permutation of the order of the extents in a single cluster becomes prohibitively expensive. Practically relevant cases where this happens have not been identified yet.

Note that it is unclear at this time how the SM2 method can be realized. A particular challenge is that a parameter vertex in the graph $\mathcal{F}$ (without observation arcs) with multiple directed paths to a single extent direction should only be counted once in a candidate subsystem. Inspiration for a solution may be drawn from sparse principal component analysis [14, 15], network component analysis [16, 17], and other sparse methods [18, 19, 20, 21].

References

[1] K. Villez, J. Billeter, and D. Bonvin. Incremental parameter estimation under rank-deficient measurement conditions. *Processes*, 7:75, 2019.

[2] J. Billeter, D. Bonvin, and K. Villez. Extent-based model identication under incomplete observability conditions. technical report no. 6, v1.0. Technical report, Eawag, 2018.

[3] J. Billeter, D. Bonvin, and K. Villez. Extent-based model identication under incomplete observability conditions. technical report no. 6, v2.0. Technical report, Eawag, 2018.

[4] N Bhatt, M Amrhein, and D Bonvin. Incremental identification of reaction and mass-transfer kinetics using the concept of extents. *Industrial & Engineering Chemistry Research*, 50(23):12960–12974, 2011.

[5] N Bhatt, N Kerimoglu, M Amrhein, W Marquardt, and D Bonvin. Incremental identification of reaction systems – A comparison between rate-based and extent-based approaches. *Chemical Engineering Science*, 83:24–38, 2012.

[6] D Rodrigues, S Srinivasan, J Billeter, and D Bonvin. Variant and invariant states for chemical reaction systems. *Computers & Chemical Engineering*, 73:23–33, 2015.

[7] A Ma*(v)* sić, J Billeter, D Bonvin, and K Villez. Extent computation under rank-deficient conditions. *IFAC-PapersOnLine*, 50:3929–3934, 2017.

[8] A Ma*(v)* sić, S Srinivasan, J Billeter, D Bonvin, and K Villez. Identification of biokinetic models using the concept of extents. *Environmental Science and Technology*, 51:7520–7531, 2017.

[9] S Srinivasan, J Billeter, S Narasimhan, and D Bonvin. Data reconciliation for chemical reaction systems using vessel extents and shape constraints. *Computers & Chemical Engineering*, 101:44–58, 2017.

[10] A. Ma*(v)* sić, K. Udert, and K. Villez. Global parameter optimization for biokinetic modeling of simple batch experiments. *Environmental Modelling and Software*, 85:356–373, 2016.

[11] D Rodrigues, J Billeter, and D & Bonvin. Maximum-likelihood estimation of kinetic parameters via the extent-based incremental approach. *Computers & Chemical Engineering*, Accepted:in Press, 2018.

[12] A. Aldroubi and A. Sekmen. Reduced row echelon form and non-linear approximation for subspace segmentation and high-dimensional data clustering. *Applied and Computational Harmonic Analysis*, 37(2):271–287, 2014.

[13] R. Vidal. Subspace clustering. *IEEE Signal Processing Magazine*, 28(2):52–68, 2011.

[14] H. Zou, T. Hastie, and R. Tibshirani. Sparse principal component analysis. *Journal of Computational and Graphical Statistics*, 15(2):265–286, 2006.

[15] A. d'Aspremont, F. Bach, and L. E. Ghaoui. Optimal solutions for sparse principal component analysis. *Journal of Machine Learning Research*, 9:1269–1294, 2008.

[16] J. C. Liao, R. Boscolo, Y. L. Yang, L. M. Tran, C. Sabatti, and V. P. Roychowdhury. Network component analysis: reconstruction of regulatory signals in biological systems. *Proceedings of the National Academy of Sciences*, 100(26):15522–15527, 2003.

[17] I. Tolle, X. Huang, Y. A. Akpalu, and L. L. Martin. A modified network component analysis (nca) methodology for the decomposition of x-ray scattering signatures. *Industrial & Engineering Chemistry Research*, 48(13):6137–6144, 2009.

[18] Y. Saad. *Iterative methods for sparse linear systems (Vol. 82)*. SIAM, 2003.

[19] T. A. Davis. *Direct methods for sparse linear systems (Vol. 2)*. SIAM, 2006.

[20] A. Bordbar. *Utilizing genome-scale models to enhance high-throughput data analysis: From pathways to dynamics*. University of California, San Diego, 2014.

[21] B. O. Palsson. *Systems Biology: Constraint-based Reconstruction and Analysis*. Cambridge University Press, 2015.